University of Groningen

Crystal structure and thermal behavior of Bi $_6$ Te $_2$ O $_{15}$

Nénert, Gwilherm; Missen, Owen P.; Lian, Hong; Weil, Matthias; Blake, Graeme R.; Kampf, Anthony R.; Mills, Stuart J.

IMPORTANT NOTE: You are advised to consult the publisher's version (publisher's PDF) if you wish to cite from it. Please check the document version below.

Document Version
Publisher's PDF, also known as Version of record

Publication date:
2020

Link to publication in University of Groningen/UMCG research database

ORIGINAL PAPER

Crystal structure and thermal behavior of $Bi_6Te_2O_{15}$: investigation of synthetic and natural pingguite

Gwilherm Nénert[1] · Owen P. Missen[2,3] · Hong Lian[4] · Matthias Weil[5] · Graeme R. Blake[4] · Anthony R. Kampf[6] · Stuart J. Mills[2]

Abstract

The previously unknown crystal structure of pingguite was determined and refined from laboratory X-ray powder diffraction data using a synthetic sample. Additional single crystal diffraction of natural pingguite confirms that the crystal structure of the synthetic sample is identical to the natural mineral. This new crystal structure calls for a revised chemistry of the rare mineral pingguite to $Bi_6Te_2O_{15}$ instead of the previously reported formula $Bi_6Te_2O_{13}$. Pingguite contains Te^{VI} only and not Te^{IV} as previously reported. Pingguite undergoes an irreversible phase transition around 840 °C which is characterized by a loss of oxygen and a reduction from Te^{VI} to Te^{IV} resulting in a δ-Bi_2O_3 like type structure. In addition, we report the Raman spectroscopic data on the natural pingguite.

Keywords Pingguite · Tellurate · Crystal structure · High-temperature transformation · Blue Bell · California · USA

Introduction

Pingguite was first reported in 1994 from the Yangjia Au deposit, Beijing municipality, China, as $Bi_6Te_2^{IV}O_{13}$ (Zhifu et al. 1994). No crystal structure was determinable and

✉ Gwilherm Nénert
gwilherm.nenert@malvernpanalytical.com

Stuart J. Mills
SMills@museum.vic.gov.au

1 Malvern Panalytical B. V., Lelyweg 1, 7602 EA Almelo, The Netherlands

2 Geosciences, Museums Victoria, GPO Box 666, Melbourne, Victoria 3001, Australia

3 School of Earth, Atmosphere and Environment, Monash University, 9 Rainforest Walk, Clayton, Victoria 3800, Australia

4 Zernike Institute for Advanced Materials, University of Groningen, Nijenborgh 4, 9747 AG Groningen, The Netherlands

5 Division of Structural Chemistry, Institute for Chemical Technologies and Analytics, Vienna University of Technology, Getreidemarkt 9/164-SC, 1060 Vienna, Austria

6 Mineral Sciences Department, Natural History Museum of Los Angeles County, 900 Exposition Boulevard, Los Angeles, CA 90007, USA

the valence of Te was determined by X-ray photoelectron spectroscopy (XPS). Subsequent occurrences of pingguite have been found in four additional countries, a more widespread distribution than many secondary tellurium minerals. Around half of the ~90 secondary Te minerals are found only in North America (Missen et al. 2020). Despite its low planetary abundance, tellurium is found in an anomalously large number of minerals (Christy 2015). This is in part due to its complex chemistry in surface environments, including the stability of two higher oxidation states (Te^{IV} and Te^{VI}) which may coexist (Missen et al. 2020). Pingguite is the most recently described mineral containing only bismuth, tellurium and oxygen, following smirnite (orthorhombic $Bi_2Te^{IV}O_5$) (Spiridonov et al. 1987; López et al. 2019) and chekhovichite (monoclinic $Bi_2Te_4^{IV}O_{11}$) (Spiridonov et al. 1987; Rossell et al. 1992). We note that smirnite and chekhovichite were structurally determined by means of only a synthetic analogue.

Additionally, pingguite is one of four secondary tellurium minerals described from China, along with chiluite ($Bi_3Te^{VI}Mo^{VI}O_{10.5}$) (Yong et al. 1989), tewite ($K_{1.5}(Te_{1.25}W_{0.25})W_5O_{19}$) (Guowu et al. 2019) and zincospiroffite ($Zn_2Te_3^{IV}O_8$) (Zhang et al. 2004). The remaining described Bi–Te–O minerals are bodieite ($Bi_2(Te^{IV}O_3)_2(SO_4)$) (Kampf et al. 2018), montanite [$Bi_2(Te^{VI}O_6)\cdot2H_2O$] and yecoraite [$Fe_3^{III}Bi_5(Te^{VI}O_4)_2(Te^{IV}O_3)O_9\cdot9H_2O$] (Williams and Cesbron 1985). We

note that chiluite ($Bi_3Te^{VI}MoO_{10.5}$), montanite ($Bi_2TeO_6 \cdot 2H_2O$) and yecoraite do not have known crystal structures, with montanite (first described in 1868) listed as having questionable status by the International Mineralogical Association (Pasero 2020). Therefore, additional investigations are necessary on Bi–Te–O-based minerals. In this contribution, we report on the structural, spectroscopic and thermal characterization of synthetic and natural pingguite.

Experimental

### Synthesis of the synthetic sample

The compound $Bi_6Te_2O_{15}$ was prepared by solid-state reaction adapting the method reported previously (Sakai et al. 1994). Starting materials were Bi_2O_3 and TeO_2 (99.9% purity). The two powders were mixed in the correct molar ratio in an agate mortar with ethanol for one hour to mix them thoroughly. After drying, the mixture was sintered in an uncovered Pt crucible at 650°C for 24 h in air and slowly cooled in the furnace.

Natural pingguite description and mineralogy

Pingguite is a very rare mineral, but exceptional specimens may be found at the Blue Bell mine, California, USA (35° 14'30" N, 116°12'16" W)—particularly near the D adit. The Blue Bell mining area formerly produced lead, copper, silver and gold, but has not been mined commercially for over 60 years (Mills et al. 2014). Pingguite from the Blue Bell area is interpreted as being formed by the oxidation of primary Bi–Te mineral phases, though few primary minerals remain due to prevailing oxidising conditions. High-quality pingguite tends to form balls of radiating, plate-like crystals up to 0.5 mm in length, with colour ranging from pale yellow to light blue and green (Fig. 1). Pingguite may also form powdery coatings when poorly crystallised.

Single crystal X-ray diffraction

Single-crystal X-ray diffraction studies on natural pingguite were carried out on a $50 \times 10 \times 5\mu m$ crystal fragment at the Natural History Museum of Los Angeles County using a Rigaku R-Axis Rapid II curved imaging plate microdiffractometer, with monochromatic MoK_α radiation. The Rigaku CrystalClear software package was used for processing the structure data, including the application of empirical multi-scan absorption corrections using ABSCOR (Higashi 2001). Structure models were obtained by the charge-flipping method using SHELXT (Sheldrick 2015a) and refinement proceeded by full-matrix least–squares on F^2 using
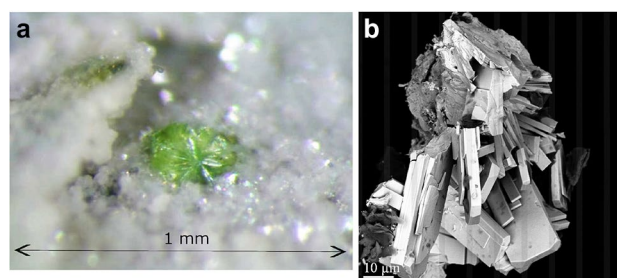
Fig. 1 (a) Optical image of pingguite from the D adit of the Blue Bell mine (specimen and photo credit: Brent Thorne; field of view: 1 mm) and (b) backscatter mode SEM image of pingguite crystals (image credit: Bob Housley)

SHELXL-2016 (Sheldrick 2015b). The highly absorbing crystals ($\mu = 84.9$ mm^{-1}) were poorly diffracting resulting in a high R_{int} of 0.14. Nevertheless, all non-oxygen sites were successfully refined with anisotropic displacement parameters; most O sites became non-positive definite when refined anisotropically, so they were refined isotropically. The final refinement resulted in an R_1 of 0.0533. Structure data were finally standardized using the Structure Tidy routine (Gelato and Parthé 1987).

Powder X-ray diffraction

High-resolution X-ray powder diffraction data for synthetic pingguite $Bi_6Te_2O_{15}$ was collected on an Empyrean Alpha-1 diffractometer using monochromatic copper Kα_1 radiation using an incident beam Johansson Ge monochromator and fixed 0.125° slits. The monochromator has already an axial divergence of about 0.02 rad and consequently only a secondary side 0.02 rad Soller slit was used. Data were collected in the angular range covering $2\theta = 15 - 100°$ with a step size of $\Delta 2\theta = 0.0066°$ and a variable counting time strategy. The XRD pattern was indexed using the program Dicvol (Boultif and Louër 2004) run in HighScore Plus 4.9 (Degen et al. 2014) via the positions of 22 diffraction peaks. It gives rise to an orthorhombic unit cell ($M(22) = 58.8$, $F(22) = 114$). The resulting unit-cell was $a \simeq 10.61$ Å, $b \simeq 22.74$ Å and $c \simeq 5.39$ Å. We note that those cell parameters are in good agreement with a previous work (Sakai et al. 1994) as well as the single crystal data for natural pingguite.

A Pawley fit with symmetry $P222$ was carried out within HighScore Plus 4.9 to extract the intensities. The space group search using the systematic absences was done using the program ExtSym (Markvardsen et al. 2008) as incorporated in the HighScore suite. A space group search suggested the space group $Pnma$ which described well the data. The structure determination was performed using the program FOX (Favre-Nicolin and Cerny 2002). Rietveld refinement was carried out to confirm the structural model determined
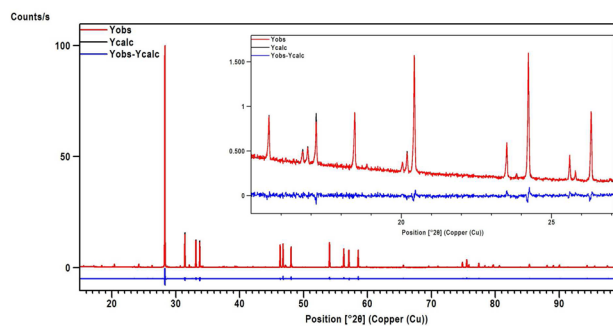
from parallel tempering. The resulting fit of the data is shown in Fig. 2 and the resulting structural details are given in Table 1. The final Rietveld refinement gives rise to a good fit of the data with reasonable statistics (R_{wp} = 6.7% and GoF = 1.8). Small amount of impurities were observed in the synthetic sample which could be identified as $\beta - Bi_2O_3$ and $\delta - Bi_2O_3$. Those phases were included in the final Rietveld refinement and the resulting quantification suggests a total impurity phase content of 0.6(2)% in weight.

The temperature dependence of synthetic $Bi_6Te_2O_{15}$ was investigated using a HTK 1200N chamber from Anton Paar in the range 25-850°C in air using copper $K\alpha_{1,2}$ radiation. At all temperatures, the sample was allowed to thermally equilibrate for few minutes prior to the start of the 13-min data collection for cell parameter determination using a Pawley fit.

Fig. 2 Rietveld refinement of $Bi_6Te_2O_{15}$ at room temperature with the symmetry *Pnma* using HighScore Plus (Degen et al. 2014). The inset shows the fit of the data in the low 2θ range emphasizing the small peaks. Statistics: R_{wp} = 6.7%, GoF = 1.8

Table 1 Crystallographic coordinates extracted from the single crystal and Rietveld refinements carried out for the natural (roman text) and synthetic (italic) pingguite using the space group *Pnma*

Atom	Wyckoff	x	y	z
Bi$_1$	8d	0.11670(15)	0.62239(8)	0.2659(2)
		0.11570(9)	*0.62244(5)*	*0.2670(2)*
Bi$_2$	8d	0.37994(15)	0.00591(7)	0.2823(3)
		0.3795(1)	*0.005860*	*0.2827(2)*
Bi$_3$	4c	0.1380(2)	$^1/_4$	0.7759(4)
		0.1403(1)	*$^1/_4$*	*0.7246(3)*
Bi$_4$	4c	0.3903(2)	$^1/_4$	0.2693(4)
		0.3898(1)	*$^1/_4$*	*0.2692(2)*
Te	8d	0.1316(2)	0.12789(14)	0.2521(4)
		0.1303(2)	*0.12817(8)*	*0.2508(2)*
O$_1$	8d	0.004(2)	0.1628(10)	0.050(4)
		0.004(1)	*0.1621(6)*	*0.041(2)*
O$_2$	8d	0.011(2)	0.0721(10)	0.388(3)
		0.014(1)	*0.0740(5)*	*0.390(2)*
O$_3$	8d	0.0627(19)	0.5324(9)	0.142(4)
		0.061(1)	*0.5332(5)*	*0.153(2)*
O$_4$	8d	0.076(2)	0.1795(11)	0.505(4)
		0.077(1)	*0.1814(5)*	*0.505(2)*
O$_5$	8d	0.2481(19)	0.1855(9)	0.124(3)
		0.248(1)	*0.1868(6)*	*0.121(2)*
O$_6$	8d	0.258(2)	0.0935(12)	0.450(4)
		0.260(1)	*0.0965(6)*	*0.455(2)*
O$_7$	8d	0.313(2)	0.5764(10)	0.498(4)
		0.305(1)	*0.5783(6)*	*0.510(2)*
O$_8$	4c	0.325(3)	$^1/_4$	0.640(5)
		0.328(1)	*$^1/_4$*	*0.639(3)*

The refined atomic coordinates for the Rietveld refinement are shown in italic. The corresponding cell parameters are, respectively, a = 10.637(2) Å, b = 22.797(4) Å, c = 5.4136(11) Å for natural pingguite and a = 10.61155(2) Å, b = 22.74458(4) Å, c = 5.399038(8) Å for the synthetic one

Corrections were applied to compensate for the height displacement due to thermal expansion of the flange used to hold the sample within the chamber. This correction was carried out by measuring the direct beam and translating the sample within the beam until complete blocking of the beam. Then the inflection point was determined automatically and the chamber with the sample was positioned at the correct height for each temperature point. This automatic correction ensures that the sample displacement is independent of temperature which is of prime importance for an accurate cell parameter determination while measuring in reflection geometry.

For the Pawley refinements, the HighScore suite was used, which allowed the refinements to proceed in batches; the results file of the previous run was taken as the seed-file for the following refinement and with the possibility to export the refined cell parameters including their error bars in ascii format.

Thermal analysis

Simultaneous thermogravimetry (TG) and differential scanning calorimetry (DSC) were used to study the change in oxygen content of the heated sample on a TG 2960 SDT instrument (Artisan Technology group) with 100 mL/min oxygen flow; the heating rate was 10°C/min over the temperature range from 30 to 1000°C.

Raman spectroscopy

A Renishaw M-1000 spectrometer with a 514-nm argon ion solid-state laser (at Division of Geological and Planetary Sciences, California Institute of Technology) was used to collect the Raman spectrum of natural pingguite. Scanning was performed at 10% power and 20 × magnification resulting in a 5 µm spot size. A polarisation scrambler was used to minimise polarisation effects and the energy scale was

calibrated with silicon at $520.5\ cm^{-1}$ and a low-wavenumber filter that allowed spectra to be recorded down to $10\ cm^{-1}$.

Results and discussion

## Crystal structure of $Bi_6Te_2O_{15}$: a new structural type

Room temperature crystal structure

$Bi_6Te_2O_{15}$ crystallizes in a new crystal structure type. We show general views of this crystal structure in Fig. 3. All the Bi atoms are surrounded by 5 nearest neighbour oxygen atoms forming irregular square pyramids. One sublattice is comprised of chains of the BiO_5 square pyramids of Bi_3 and Bi_4 running along the c-direction. The square pyramids point alternately up and down, as illustrated in Figure 4a). They are forming chains consisting of edge- and corner-sharing square pyramids, which are running along the c-direction. The square pyramids of Bi_1 and Bi_2 form a ladder network which is located above the square pyramids chains made of Bi_3 and Bi_4 along the b-direction. This is illustrated in Fig. 4b). Between this ladder network and those zigzag chains, there are voids in the structure containing the TeO_6
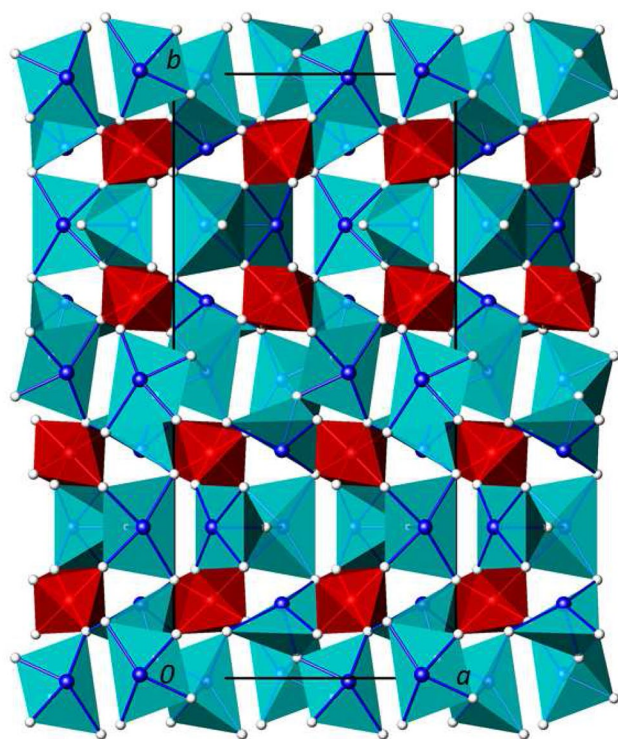
Fig. 3 Crystal structure of pingguite projected along the c axis. The Te atom has an octahedral environment while all Bi atoms are coordinated in square pyramidal fashion. Figure generated with ATOMS (Shape Software)
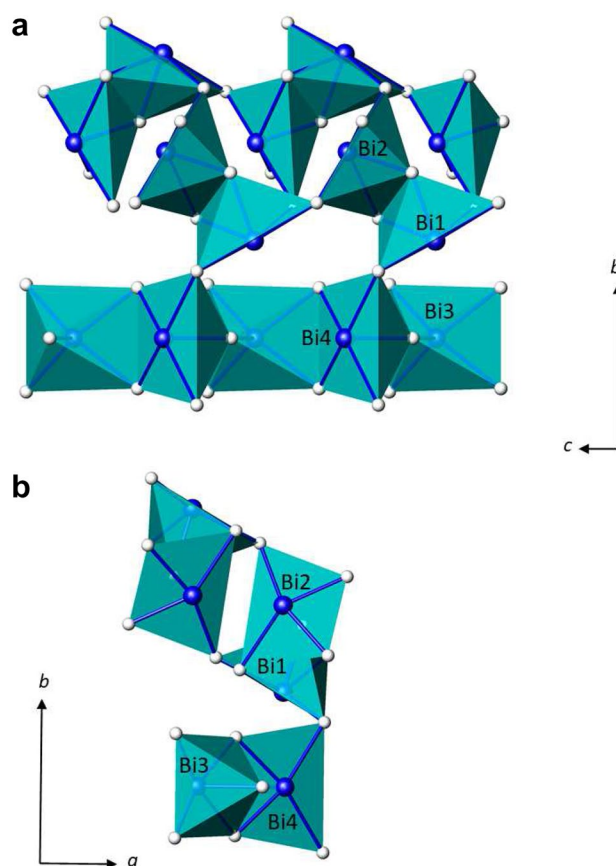
Fig. 4 a Network of BiO_5 square pyramids projected along the a axis and **b** along the c axis. For clarity, the Te atoms have been disregarded in these representations. Figure generated with ATOMS (Shape Software)

octahedra (see Fig. 3). The $6s^2$ electron lone pairs situated at the Bi^{III} atoms are stereochemically active and protrude into the remaining voids of the structure.

Selected bond lengths obtained from the refinement are given in Table 2. We note that the TeO_6 octahedra are very regular within the reported error bars. The volume of the square pyramids varies between 6.9 and 8.4 $Å^3$.

To confirm our structural analysis, we have made a bond-valence analysis, presented in Table 3. For this purpose, we used the parameters of Mills and Christy (2013) for Te^{VI}–O bonds and Krivovichev (2012) for Bi^{III}–O bonds. The bond-valence analysis suggests that a few secondary Bi–O bonds are relevant to the Bi coordination environments.

Discussion about the oxidation state of tellurium in pingguite

Using chemical analysis, Zhifu et al. (1994) reported a ratio Bi:Te = 3:1. In the absence of a structural model, they used XPS measurement to tentatively identify the oxidation state

Table 2 Selected bond lengths (in Å), respectively, for natural (single-crystal X-ray diffraction) and synthetic pingguite (powder X-ray diffraction, in italic) as extracted from single crystal and Rietveld refinements of X-ray diffraction data

Te-O_1	1.92(3)	Bi_2-O_2	2.25(3)
	1.92(1)		*2.30(1)*
Te-O_2	1.95(3)	Bi_2-O_3	2.13(3)
	1.90(1)		*2.15(1)*
Te-O_4	1.90(3)	Bi_2-O_3	2.17(3)
	1.92(1)		*2.19(1)*
Te-O_5	1.93(3)	Bi_2-O_6	2.55(3)
	1.95(1)		*2.59(1)*
Te-O_6	1.89(3)	Bi_2-O_7	2.32(3)
	1.91(1)		*2.36(1)*
Te-O_7	1.90(3)	Bi_3-O_4	2.27(3) × 2
	1.94(1)		*2.24(1) × 2*
Bi_1-O_1	2.33(3)	Bi_3-O_5	2.662(19) × 2
	2.28(1)		*2.62(1) × 2*
Bi_1-O_2	2.58(2)	Bi_3-O_8	2.12(4)
	2.55(1)		*2.12(2)*
Bi_1-O_3	2.23(3)	Bi_4-O_1	2.52(3) × 2
	2.20(1)		*2.55(1) × 2*
Bi_1-O_6	2.27(3)	Bi_4-O_5	2.25(2) × 2
	2.22(1)		*2.23(1) × 2*
Bi_1-O_7	2.65(3)	Bi_4-O_8	2.12(3)
	2.55(1)		*2.10(2)*

of tellurium and from there suggested a chemical formula $Bi_6Te_2O_{13}$ for pingguite. The measured core level Te $3d_{5/2}$ peak was 576 eV. The authors reported that the theoretical value of the core level Te $3d_{5/2}$ peak for Te^{IV} was 576 eV while for Te^{VI} it was 577 eV. Based on this difference, they assigned the oxidation state IV to the tellurium atom in pingguite. However it should be noted that this evidence for Te^{IV} is weak. Indeed, most of XPS spectrometers have an energy resolution of about 1 eV, consequently, it becomes difficult to assign a measured core level peak at 576 eV to Te^{IV} with a high level of confidence . Additionally, depending on the chemical environment of the Te^{IV}, this associated core level

energy can vary by more than 1 eV (Wagner 1991). Consequently, the reported XPS data by Zhifu et al. (1994) are not in disagreement with the existence of a tellurium ion with an oxidation state of VI.

The regularity of the TeO_6 octahedra in pingguite shows that Te is in the VI valence state rather than IV. $Te^{IV}O_6$ octahedra tend to display high levels of distortion (Christy and Mills 2013), with three short bonds (less than 1.95 Å) to oxygen and three long bonds (usually greater than 2.70 Å), distortion which is not observed in the structure of pingguite. As a result, the bond-valence sum for the Te site is 6.06 valence units (vu), i.e. confirming that Te is present in pingguite as Te^{VI} (see Table 3).

High-temperature behavior

Thermal analysis study and nature of the high-temperature phase

As the initial work on pingguite reported an anomaly in the DTA measurement somewhere above 800°C (Zhifu et al. (1994)), we have carried out a DSC/TGA experiment on synthetic pingguite to probe the possible existence of a phase transition above room temperature. We show in Fig. 5 the obtained measurements. A clear anomaly is observed around 845 °C in the DSC signal which is concomitant with a mass loss of about 1.88%, which perfectly fits with a release of one oxygen molecule per formula unit (theoretical mass loss value: 1.83%) and a corresponding reduction of the oxidation state of tellurium from Te^{VI} to Te^{IV}, resulting in a high temperature phase of $Bi_6Te_2O_{13}$. It has been shown that actually this phase can be stabilized at room temperature by quenching from the high temperature phase as reported by Sakai et al. (1994).

To gain further insight into the nature of the high temperature phase, we have carried out high temperature diffraction at 855 °C. The observed phase is a cubic phase characterized by $a = 5.68306(6)$ Å and space group $Fm\overline{3}m$ corresponding to the δ-Bi_2O_3 structure type. To fit the experimental pattern, we used the disordered model proposed by Battle

Table 3 Bond-valence sum analysis of natural pingguite

	Bi_1	Bi_2	Bi_3	Bi_4	Te	Σ
O_1	0.49	–	0.16	0.33	1.00	1.99
O_2	0.29	0.58, 0.12	–	–	0.95	1.94
O_3	0.61	0.75, 0.69	–	–	–	2.04
O_4	0.21	–	0.56	0.14	1.04	1.95
O_5	0.18	–	0.25	0.58	0.98	1.99
O_6	0.56	0.31,0.07	–	–	1.06	2.00
O_7	0.25	0.50, 0.11	–	–	1.04	1.91
O_8	0.11	- -	0.76,0.06	0.76	–	1.69
Σ	2.71	3.14	2.76	2.86	6.07	–
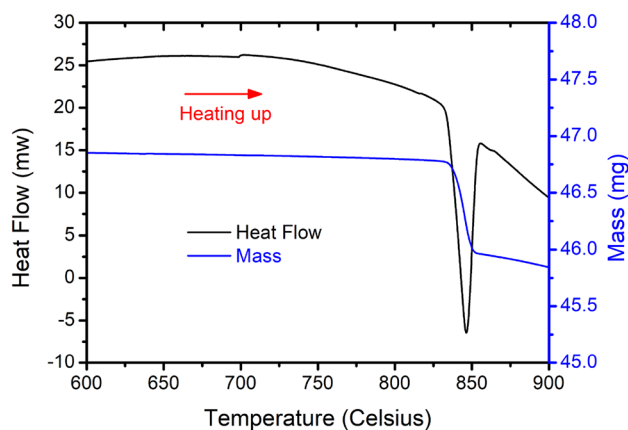
Fig. 5 Thermogravimetric and calorimetric evolution of the synthetic $Bi_6Te_2O_{15}$. The peak in the DSC signal around 845 °C corresponds to a release of oxygen resulting in a phase $Bi_6Te_2O_{13}$ above this temperature
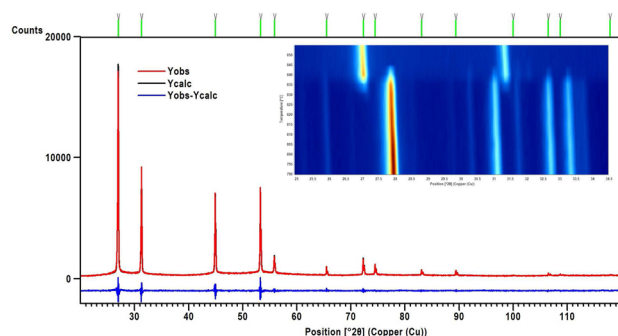
Fig. 6 Rietveld refinement of the high temperature cubic phase exhibiting the δ-Bi_2O_3 structure. The inset shows an isoline plot illustrating the first order phase transition with the phase coexistence between the pingguite orthorhombic phase and the high temperature cubic phase $Bi_6Te_2O_{13}$. Statistics: R_{wp} = 7.7% and GoF = 1.6

Table 4 Crystallographic coordinates extracted from the Rietveld refinement carried out on powder X-ray diffraction data using the space group $Fm\overline{3}m$ (No 225) at 855 °C with cell parameters $a=$ 5.68306(6) Å for $Bi_6Te_2O_{13}$

Atom	Wyckoff	x	y	z	Occ
Bi_1	4a	0	0	0	$\frac{3}{4}$
Te_1	4a	0	0	0	$\frac{1}{4}$
O_1	8c	$\frac{1}{4}$	$\frac{1}{4}$	$\frac{1}{4}$	0.43
O_2	32f	0.403(2)	0.403(2)	0.403(2)	0.095

Fig. 7 Relative expansion of synthetic pingguite. Variation of cell parameters normalized to values at 25 °C as a function of temperature. The solid line is the best fit of the data to Eq. (1)
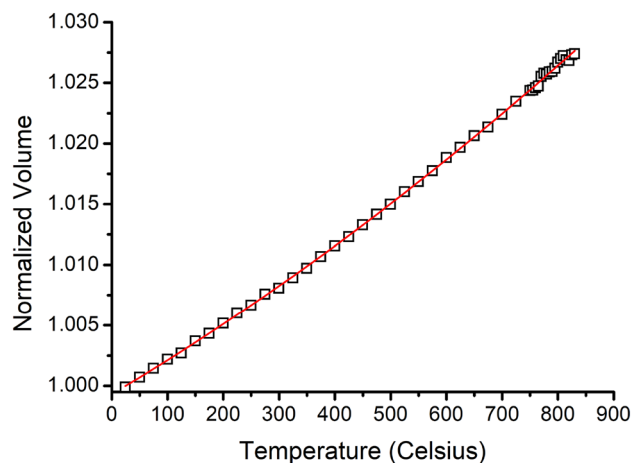
et al. (1983) where we have adjusted the occupation of the Wyckoff positions 32f and 8c. The best fit which could be obtained is shown in Fig. 6 and the corresponding refined parameters are given in Table 4.

Thermal expansion of synthetic pingguite

The values of the cell parameters as a function of temperature are plotted in Fig. 7. The synthetic pingguite shows a quasi-linear variation of the cell parameters as a function of temperature with little curvature. The temperature evolution of the b cell parameter is slightly different from a and c resulting in a low thermal expansion anisotropy. To quantify the expansivity of the pingguite, we used the program EosFit (Angel et al. 2014). The various fits were obtained using the second-order polynomial thermal expansion equation proposed by Berman (1988):

$$L(T) = L_{25}\left[1 + \alpha_0\left(T - T_{25}\right) + \alpha_1\left(T - T_{25}\right)^2\right], \quad (1)$$

where L refers to volume or cell parameter and from which one can obtain the linear thermal expansion:

$$\frac{\partial L}{\partial T} = \alpha_{L,T} = \alpha_0 + 2\alpha_1\left(T - T_{25}\right). \quad (2)$$

We present, respectively, in Figs. 7 and 8, the resulting fit of the thermal expansion of the unit-cell volume and of the cell parameters. From those fits, one can extract the volumetric thermal expansion α_V and the linear thermal expansion coefficient $\alpha_i (i = 1$–$3)$ along the principal crystallographic axes. The various α_0 and α_1 are reported in Table 5. The quality of the extracted values is confirmed by the excellent agreement between $\sum_{n=1}^{3} \alpha_{ii}$ with α_V as the expected relationship is $\alpha_V = \alpha_{11} + \alpha_{22} + \alpha_{33}$ for an orthorhombic cell.

We note that pingguite exhibits a linear thermal expansion which is almost twice as small as the thermal expansion reported for other Te based minerals such as tellurobismuthite (Pavlova et al. 2011). In addition, despite the considerably different unit-cell parameters, the thermal expansion of
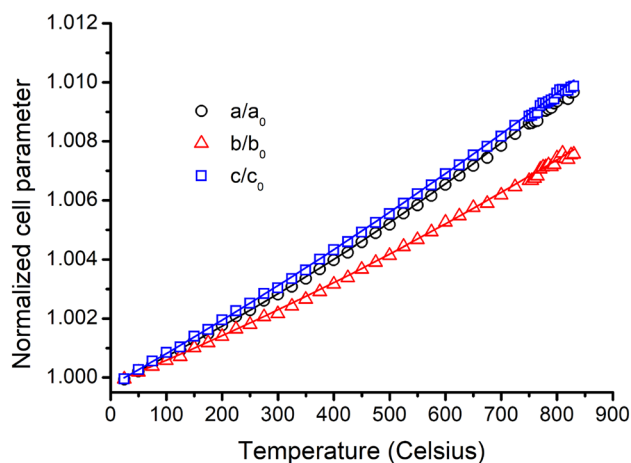
Fig. 8 Relative expansion of synthetic pingguite. Variation of the volume normalized to values at 25 °C as a function of temperature. The curve is the best fit of the data to Eq. (1)

Table 5 Volumetric linear thermal expansion and linear thermal expansion coefficients $\alpha_i (i = 1-3)$ along the principal crystallographic axes obtained using the Berman (1988) equation (see Eq. 2 for α_0 and α_1)

Component	α_0 ($\times 10^{-5}$ K^{-1})	α_1 ($\times 10^{-8}$ K^{-2})
α_{11}	0.93(1)	0.72(2)
α_{22}	0.77(1)	0.46(4)
α_{33}	1.07(1)	0.44(2)
α_V	2.77(4)	1.64(8)
$\sum_{n=1}^{3} \alpha_{ii}$	2.77(3)	1.62(8)

pingguite is not very anisotropic with α_{11} being very similar to α_{33}.

Raman spectroscopy

We present in Fig. 9, the Raman spectrum recorded on natural pingguite. The spectrum shows the presence of octahedral TeO_6^{6-} anions in pingguite and confirms that pingguite is an anhydrous mineral. The spectrum is relatively complicated due to the presence of minor impurities. Above 1500 cm^{-1}, the spectrum is flat, indicating that there are no O–H or H_2O groups present in pingguite, consistent with the crystal structure. The orthotellurate band (the symmetric v_1 stretching mode of the octahedral TeO_6^{6-} anion) is centred on 730 cm^{-1}, similar to the major tellurate bands in the tellurate minerals bairdite (721 cm^{-1}; Kampf et al. 2013a) and eckhardite (729 cm^{-1}; Kampf et al. 2013b). The major tellurite (Te^{IV}-O) stretching mode tends to have a higher Raman shift than the stretching mode of tellurate (e.g. 761 cm^{-1} in bodieite; Kampf et al. 2018), further evidence that the Te in pingguite is
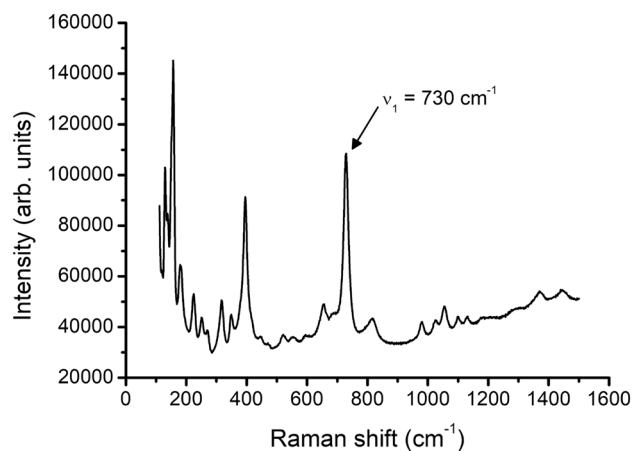
Fig. 9 Raman spectrum of natural pingguite. The major tellurate symmetric v_1 stretching mode is centred on 730 cm^{-1}

Te^{VI}. The antisymmetric v_3 stretching mode of the tellurate anion is centred on 662 cm^{-1}. Peaks below 500 cm^{-1} are attributable to bending modes of the tellurate anion, Bi–O modes and lattice modes.

Conclusion

We have precisely determined the crystal structure of synthetic and natural pingguite for the first time, along with the thermal behavior of this bismuth tellurate. The crystal structure determination of the natural pingguite confirmed by the synthetic sample calls for a redefinition of the chemical formula of this rare mineral. The chemical formula is $Bi_6Te_2O_{15}$ evidencing the presence of Te^{VI} and not Te^{IV} as initially reported. Its thermal expansion shows that it exhibits a low thermal anisotropy prior to undergoing an irreversible phase transition around 840 °C towards a δ-Bi_2O_3-type phase with mixed occupancy of Te and Bi atoms, concomitant with a release of oxygen leading to the formula $Bi_6Te_2^{IV}O_{13}$.

References

Angel RJ, Gonzalez-Platas J, Alvaro M (2014) EosFit-7c and a Fortran module (library) for equation of state calculations. Z Kristallogr 229:405–419. https://doi.org/10.1515/zkri-2013-1711

Battle PD, Catlow CRA, Drennan J, Murray AD (1983) The structural properties of the oxygen conducting δ phase of Bi_2O_3. J Phys C 16:L561. https://doi.org/10.1088/0022-3719/16/17/003

Berman RG (1988) Internally-consistent thermodynamic data for minerals in the system $Na_2O - K_2O - CaO - MgO - FeO - Fe_2O_3 - Al_2O_3 - SiO_2 - TiO_2 H_2O - CO_2$. J Petrol 29:445–522. https://doi.org/10.1093/petrology/29.2.445

Boultif A, Louër D (2004) Powder pattern indexing with the dichotomy method. J Appl Cryst 37:724–731. https://doi.org/10.1107/S0021889804014876

Christy AG, Mills SJ (2013) Effect of lone-pair stereoactivity on polyhedral volume and structural flexibility: Application to $Te^{IV}O_6$ octahedra. Acta Crystallogr B69:446–456. https://doi.org/10.1107/S2052519213023087

Christy AG (2015) Causes of anomalous mineralogical diversity in the periodic table. Mineral Mag 79:33–50. https://doi.org/10.1180/minmag.2015.079.1.04

Christy AG, Mills SJ, Kampf AR (2016) A review of the structural architecture of tellurium oxycompounds. Mineral Mag 80:415–545. https://doi.org/10.1180/minmag.2016.080.093

Degen T, Sadki M, Bron E, König U, Nénert G (2014) The HighScore suite. Powder Diffract 29(S2):S13–S18. https://doi.org/10.1017/S0885715614000840

Favre-Nicolin V, Cerny R (2002) FOX, 'free objects for crystallography': a modular approach to ab initio structure determination from powder diffraction. J Appl Cryst 35:734–743. https://doi.org/10.1107/S0021889802015236

Gelato LM, Parthé E (1987) J Appl Cryst 20:139–143. https://doi.org/10.1107/S0021889887086965

Guowu L, Yuan X, Ming X (2019) Tewite: a K-Te-W new mineral species with a modified tungsten-bronze type structure, from the Panzhihua-Xichang region, southwest China. Eur J Mineral 31(1):145–152. https://doi.org/10.1127/ejm/2019/0031-2813

Higashi T (2001) ABSCOR. Rigaku Corporation, Tokyo

Kampf AR, Mills SJ, Housley RM, Rossman GR, Marty J, Thorne B (2013a) Lead-tellurium oxysalts from Otto Mountain near Baker, California: X. Bairdite, $Pb_2 Cu_4^{II}Te_2^{VI}O_{10}(OH)_2(SO_4)(H_2O)$, a new mineral with thick HCP layers. Am Mineral 98:1315–1321. https://doi.org/10.2138/am.2013.4389

Kampf AR, Mills SJ, Housley RM, Rossman GR, Marty J, Thorne B (2013b) Lead-tellurium oxysalts from Otto Mountain near Baker, California: XI. Eckhardite, $(Ca, Pb)Cu^{II} Te^{VI}O_5(H_2O)$, a new mineral with HCP stair-step layers. Am Mineral 98:1617–1623. https://doi.org/10.2138/am.2013.4529

Kampf AR, Housley RM, Rossman GR, Marty J, Chorazewicz M (2018) Bodieite, $Bi_2^{III}(Te^{IV}O_3)_2(SO_4)$, a New Mineral from the Tintic District, Utah, and the Masonic District, California, USA. Can Mineral 56:1–10. https://doi.org/10.3749/canmin.1800046

Krivovichev SV (2012) Derivation of bond-valence parameters for some cation-oxygen pairs on the basis of empirical relationships between r0 and b. Z Kristallogr Crystal Mater 227:575–579. https://doi.org/10.1524/zkri.2012.1469

López CA, Baati E, Fernández-Díaz MT, Saouma FO, Jang JI, Alonso JA (2019) Crystal structure and second harmonic generation in Bi_2TeO_5: An X-N study from synchrotron and neutron diffraction data. J Solid State Chem 276:122–127. https://doi.org/10.1016/j.jssc.2019.04.035

Markvardsen AJ, Shankland K, David WIF, Johnston JC, Ibberson RM, Tucker M, Nowell H, Griffin T (2008) ExtSym: a program to aid space-group determination from powder diffraction data. J Appl Cryst 41:1177–1181. https://doi.org/10.1107/S0021889808031087

Mills SJ, Christy AG (2013) Revised values of the bond-valence parameters for $Te^{IV} - O$, $Te^{VI} - O$ and $Te^{IV}Cl$. Acta Crystallogr B69:145–149. https://doi.org/10.1107/S2052519213004272

Mills SJ, Kampf AR, Christy AG, Housley RM, Rossman GR, Reynolds RE, Marty J (2014) Bluebellite and mojaveite, two new minerals from the central Mojave Desert, California, USA. Mineral Mag 78:1325–1340. https://doi.org/10.1180/minmag.2014.078.5.15

Missen OP, Ram R, Mills SJ, Etschmann B, Reith F, Shuster J, Smith DJ, Brugger J (2020) Love is in the Earth: a review of tellurium (bio)geochemistry in surface environments. Earth-Sci Rev 204:103150. https://doi.org/10.1016/j.earscirev.2020.103150

Pasero M (2020) The new IMA list of minerals. http://cnmnc.main.jp/

Pavlova LM, Shtern YI, Mironov RE (2011) Thermal expansion of bismuth telluride. High Temp 49:369–379. https://doi.org/10.1134/S0018151X1103014X

Rossell H, Leblanc M, Ferey G, Bevan D, Simpson D, Taylor M (1992) On the crystal structure of $Bi_2Te_4O_{11}$. Aust J Chem 45(9):1415–1425. https://doi.org/10.1071/CH9921415

Sakai H, Yamamoto M, Nakashima S, Maeda Y (1994) Investigation of a high-temperature phase of $3Bi_2O_3.2TeO_2$ binary oxide. Hyperfine Interact 90:401–405. https://doi.org/10.1007/BF02069146

Sheldrick GM (2015a) SHELXT-integrated space-group and crystal-structure determination. Acta Crystallogr A71:3–8. https://doi.org/10.1107/S2053273314026370

Sheldrick GM (2015b) Crystal structure refinement with SHELXL. Acta Crystallogr C71:3–8. https://doi.org/10.1107/S2053229614024218

Spiridonov E, Demina L (1984) Smirnite-Bi_2TeO_5, a new mineral. Dokl Akad Nauk SSSR 278(1):199–202

Spiridonov E, Petrova I, Demina L, Antonyan G (1987) Chekhovichite-$Bi_2Te_4O_{11}$, a new mineral. Vestnik Moskovskogo Univ Geol 42(6):71–76

Wagner CD (1991) The NIST X-ray photoelectron spectroscopy (XPS) database. National Institute of Standards and Technology, Gaithersburg

Williams SA, Cesbron FP (1985), Yecoraite $Fe_3Bi_5(TeO_3)(TeO_4)_2 O_9 \cdot nH_2O$ a new mineral from Sonora, Mexico. Boletín Mineral 1:10–16

Yong X, Li D, Wang G, Deng M, Chen N, Wang S (1989) A study of chiluite-a new mineral found in Chilu, Fujian. China Acta Miner Sin 9:9–14

Zhang P-H, Zhu J-C, Zhao Z-H, Gu X-P, Lin J-F (2004) Zincospiroffite, a new tellurite mineral species from the Zhongshangou Gold Deposit, Hebei Province, People's Republic of China. Can Mineral 42(3):763–768. https://doi.org/10.2113/gscanmin.42.3.763

Zhifu S, Keding L, Falan T, Jingyi Z (1994) Pingguite: a new bismuth tellurite mineral. Acta Mineral Sin 14:315